On the usefulness of the height-difference-autocorrelation function for contact mechanics

Anle Wang[1,2] and Martin H. Müser[2]

[1] *INM – Leibniz Institute for New Materials, Campus D2 2, 66123 Saarbrücken, Germany*

[2] *Department of Materials Science and Engineering, Saarland University, Campus, 66123 Saarbrücken, Germany*

Abstract

We show that various quantities of relevance to the contact mechanics of randomly rough surfaces can be directly estimated from the easy-to-acquire height-difference-autocorrelation function $G_{\delta h}(\Delta r)$. These include the areal elastic energy density and the stress autocorrelation function, for which we derive expressions that are exact for full contact (within linear elasticity) and approximate for partial contact (within Persson theory). Our approach makes it possible to estimate scale–dependent contact areas, stresses, stress gradients, or to make well-informed corrections to the Dahlquist criterion for adhesion with elementary mathematical operations that do not necessitate the Fourier transform to be taken.

Keywords: contact mechanics, self-affine surfaces, surface spectra, Persson theory

1. Introduction

Traditionally, roughness of nominally flat surfaces is characterized by the height-distribution function, also known as Abbott-Feierstone or bearing area curve [1], or by its first few moments: root-mean-square height, skewness, and kurtosis. However, their knowledge hardly provides useful information for contact mechanics. In order to make predictions on quantities like real contact area,

contact stiffness, or the mean gap as a function of load, an additional spatial characterization [2] is required. In particular, it is crucial to know to what extent roughness decomposes into long or short wavelength modes [3, 4, 5]. Predictive theoretical and computational approaches to contact mechanics are therefore based on height spectra $C_h(q)$ rather than on moments of the height distribution function [4, 6, 7]. While reporting surface-roughness spectra is now more common than in the past [5, 8], little to nothing is generally done with $C_h(q)$ beyond its reporting. Exceptions to this claim do not go much beyond — if at all — Persson theory [4, 6, 9, 10, 11] and numerical simulations [12, 13, 14, 15, 16, 17] taking $C_h(q)$ as input.

As is the case for other stationary random variables, spatial (or temporal) correlations of the height can also be expressed in real space (time) rather than in the wave vector (frequency) domain [18, 19]. In fact, the height-difference autocorrelation function (ACF)

$$G_{\delta h}(\Delta\mathbf{r}) \equiv \frac{1}{2}\left\langle \{h(\mathbf{r}) - h(\mathbf{r}+\Delta\mathbf{r})\}^2 \right\rangle, \tag{1}$$

contains the same stochastic information on the surface profile as $C_h(\mathbf{q})$. Here, $h(\mathbf{r})$ is the height as a function of the in-plane coordinate $\mathbf{r}$, while $\langle \dots \rangle$ represents an average, which is taken either over a sufficiently large sample or over a periodically repeated domain. The factor $1/2$ was introduced on the right-hand side of Eq. (1) to turn $G_{\delta h}(\Delta r)$ into a scale-dependent height variance yielding the mean-square height at large Δr.

One might conclude that knowing $G_{\delta h}(\Delta r)$ does not bear any advantage over knowing $C_h(q)$. However, it is rarely exploited that deducing $G_{\delta h}(\Delta\mathbf{r})$ from a measured height profile is much simpler than constructing $C_h(\mathbf{q})$. More importantly, it appears to have remained unnoticed how easily central tribological quantities can be deduced directly from $G_{\delta h}(\Delta\mathbf{r})$ with quite elemental mathematical operations. These quantities include the energy to fully – or locally – conform an elastic manifold to a rigid, rough substrate, scale-dependent contact stresses, and the stress-autocorrelation function. Knowledge of these quantities then allows conclusions to be drawn on the tackiness of objects or the amount

of plastic deformation.

In this article, we derive formulae that allow several tribological quantities to be calculated directly from the height-difference ACF and demonstrate their application in a few selected cases. We describe partial contact using a real-space interpretation of Persson theory, which can be advantageous for the description of heterogeneous surfaces or multi-scale approaches. While the derivations require some mathematical background, final expressions can be used with the mathematical toolbox provided at the undergraduate level in engineering.

The remainder of this paper is organized as follows: Derivations are presented in Section 2, where we first treat full and then partial contact. Section 3 demonstrates how to use the results. Conclusions are drawn in section 4.

2. Theory

2.1. Notation, definitions, and conventions

Throughout this work, we consider linear elasticity in the small-slope approximation. It allows us to distribute the combined compliance and the combined roughness arbitrarily to either side of the interface [20]. The (inverse) combined compliance is summarized in the contact modulus E^*, while $h(\mathbf{r})$ contains the combined roughness of the two surfaces. The calculations are conducted in the spirit that an ideally flat, elastic manifold is pressed against an ideally rigid, corrugated counter face. However, the calculations apply in the same fashion to a mechanical interface that is self mated in the sense that the elastic properties of the two solids in contact as well as their surface spectra are identical. In that case $h(\mathbf{r})$ should be interpreted as the interfacial separation between the two solids before they deform.

In this work, functions may be "overloaded", which means that the precise definition of a function depends on its variable. For example, $C_h(\mathbf{q})$ denotes the height spectrum at a given wave vector, while $C_h(q)$ is the average over all $C_h(\mathbf{q})$ at fixed magnitude of $\mathbf{q}$. A similar comment applies to $G_{\delta h}(\mathbf{r})$. In this context, we wish to mention that our assumption of isotropy, which we make

throughout this manuscript, can be used unless the stochastic properties of the surface profiles and elasticity are simultaneously unisotropic. In this last case, our treatment would necessitate alterations, which are straightforward to make but heavy on the book keeping of indices. We therefore see the description of simultaneous anisotropy of roughness and elasticity beyond the scope of this article.

It is often easiest to start the analysis on periodically repeated domains, in which case the height $h(\mathbf{r})$ can be represented as a complex Fourier sum according to

$$h(\mathbf{r}) \quad = \quad \sum_{\mathbf{q}} \tilde{h}(\mathbf{q}) \, \exp(i\mathbf{q} \cdot \mathbf{r}), \tag{2}$$

where $\mathbf{q}$ is a wave vector defined in the xy plane. The (mean) surface normal is taken to be parallel to the z axis and the coordinate system is chosen such that the mean height satisfies $\tilde{h}(0) = 0$. The inverse transform then reads

$$\tilde{h}(\mathbf{q}) = \frac{1}{A} \int d^2r \, h(\mathbf{r}) \, \exp(-i\mathbf{q} \cdot \mathbf{r}), \tag{3}$$

A being the area of the periodically repeated domain. One can now define the height spectrum

$$C_h(q) \equiv A \left\langle |\tilde{h}(\mathbf{q})|^2 \right\rangle, \tag{4}$$

where the expectation value on the right-hand-side of the equation should be interpreted as a disorder average over many surfaces that are generated with identical stochastic rules, or, alternatively, as a local average of $|\tilde{h}^2(\mathbf{q})|$ over different wave vectors of magnitude close to q. The tilde, which usually indicates the Fourier transform, is omitted for spectra like $C_h(\mathbf{q})$, in order to follow usual conventions. The transition from conducting a calculation on a finite domain to that on an infinite domain is achieved with the substitution $\sum_{\mathbf{q}} ... \rightarrow \{A/(2\pi)^2\} \int d^2q ....$

2.2. Relations between spectra and real-space ACFs

Before addressing contact mechanics, we recapitulate some relations between the real-space ACF of a random variable defined on a two-dimensional surface

and the corresponding spectrum. We use the height as random variable, but the equations also hold for other spatially fluctuating fields such as the normal stress. Part of the goal is to provide the reader with expressions that are not only mathematically correct but also numerically stable.

Given the definition of $G_{\delta h}(\Delta\mathbf{r})$ in the introduction, it follows that

$$\begin{aligned} G_{\delta h}(\Delta\mathbf{r}) &= \sigma_h^2 - \langle h(\mathbf{r})h(\mathbf{r}+\Delta\mathbf{r})\rangle & (5)\\ &= \sigma_h^2 - G_h(\Delta\mathbf{r}), & (6)\end{aligned}$$

where σ_h^2 is the standard deviation of the surface height, and $G_h(\Delta\mathbf{r})$ the height ACF. Expressing $h(\mathbf{r})$ via their Fourier transform leads to

$$\begin{aligned} G_{\delta h}(\Delta r) &= \sigma_h^2 - \frac{1}{A}\sum_{\mathbf{q}} C_h(q) e^{i\mathbf{q}\cdot\Delta\mathbf{r}}, & (7)\\ &\to \sigma_h^2 - \frac{1}{2\pi}\int dq\, q\, C_h(q)\, J_0(q\Delta r). & (8)\end{aligned}$$

For non-isotropic surfaces, we imply an average over all possible orientations of $\Delta\mathbf{r}$ at a fixed magnitude Δr, whenever we consider a correlation function that only depends on the magnitude of the distance, as in Eq. (7).

Since the evaluation of $G_{\delta h}(\Delta r)$ at small Δr with equation (8) requires the difference between two large numbers to be taken, it is convenient to rewrite it as

$$G_{\delta h}(\Delta r) = \frac{1}{2\pi}\int dq\, q\, C(q)\, \{1 - J_0(q\Delta r)\} \qquad (9)$$

for a numerical evaluation of $G(\Delta r)$ from $C(q)$.

Eq. (8) can be inverted for $C_h(q)$ with the Hankel transform

$$C_h(q) = 2\pi \int d\Delta r\, \Delta r J_0(q\Delta r) \left\{\sigma_h^2 - G_{\delta h}(\Delta r)\right\}. \qquad (10)$$

This time, numerical round-off errors become relevant when $G(\Delta r) \ll \sigma_h^2$ in the integrand of of equation (10). One might therefore consider to evaluate the two terms in the integrand of equation (10) separately for $\Delta r \le 1/q_\mathrm{r}$ and $\Delta r > 1/q_\mathrm{r}$, where q_r is the roll-off wave number introduced later in section 3.3. This yields

$$\begin{aligned} \frac{C_h(q)}{2\pi} &= \frac{\sigma_h^2}{q\, q_\mathrm{r}} J_1(q/q_\mathrm{r}) - \int_0^{1/q_\mathrm{r}} d\Delta r\, \Delta r J_0(q\Delta r) G_{\delta h}(\Delta r) \\ &\quad + \int_{1/q_\mathrm{r}}^{\infty} d\Delta r\, \Delta r J_0(q\Delta r) \left\{\sigma_h^2 - G_{\delta h}(\Delta r)\right\}. \qquad (11)\end{aligned}$$

Note that we have not made the assumption of the random-phase approximation in the calculation of the two-point correlation function. The formulae are therefore also valid for surfaces with correlated or deterministic roughness. A similar comment applies to all full-contact calculations presented in this study as long as the surface topography and/or the elastic properties are (statistically) isotropic.

2.3. Areal elastic-energy density in full contact

In this section, the relation between an isotropic height-difference ACF and the full-contact, areal elastic-energy density is derived in a real-space representation. The considered energy density of a periodically repeated domain is given by

$$v_{\mathrm{el}} = \sum_{\mathbf{q}} \frac{qE^*}{4} |\tilde{h}(\mathbf{q})|^2 \tag{12}$$

$$\rightarrow \int_{0^+}^{\infty} d^2q \frac{qE^*}{4} C_h(\mathbf{q}). \tag{13}$$

Replacing $C_h(\mathbf{q})$ with $-C_{\delta h}(\mathbf{q})$ for $q \neq 0$, see Eq. (6), and using the (continuous) Fourier transform to relate the height-difference spectrum $C_{\delta h}(\Delta r)$ with the height-difference ACF,

$$G_{\delta h}(\Delta \mathbf{r}) = \frac{1}{(2\pi)^2} \int d^2q e^{i\mathbf{q}\cdot\Delta\mathbf{r}} C_{\delta h}(\mathbf{q}) \tag{14}$$

$$C_{\delta h}(\mathbf{q}) = \int d^2\Delta r e^{-i\mathbf{q}\cdot\Delta\mathbf{r}} G_{\delta h}(\Delta \mathbf{r}), \tag{15}$$

the areal energy density in full contact can be written as

$$v_{\mathrm{el}} = \beta \frac{E^*}{4} \int_0^{\infty} d\Delta r \frac{G_{\delta h}(\Delta r)}{\Delta r^2} \tag{16}$$

with the dimensionless number

$$\beta \equiv -\frac{1}{2\pi} \int_0^{2\pi} d\varphi \int dq\, q^2\, e^{iq\Delta r \cos\varphi}\, q\Delta r^3$$

$$= -1 \int_0^{\infty} dx\, x^2\, J_0(x), \tag{17}$$

where $J_0(x)$ is a Bessel function of the first kind. The latter integral needs to be converted into a convergent one, which we achieve by multiplying the integrand

with a regularizing factor $\exp(-\alpha x^2)$ and by considering the limit $\alpha \to 0$. This leads us to

$$\beta = -\lim_{\alpha\to 0}\int_0^\infty dx\; x^2\; J_0(x)\exp(-\alpha x^2), \tag{18}$$

$$= 1. \tag{19}$$

In Appendix Appendix A, we show an alternative derivation for the dependence of $v_{\rm el}$ on $G_{\delta h}(\Delta r)$, which does not necessitate a regularizing function in the integral. It is based on dimensional analysis and single-wavelength roughness.

If we now consider self-affine scaling, $G_{\delta h}(\Delta r) \propto \Delta r^{2H}$, H being the Hurst roughness exponent, a well-known result can be readily recuperated: the elastic energy in full contact is dominated by large-lengthscale ondulations if $H > 0.5$ and by short lengthscales for $H < 0.5$, since the integrand in Eq. (16) scales as Δr^{2H-2}.

2.4. Stress-autocorrelation function in full contact

The stress ACF is defined as

$$G_\sigma(\Delta\mathbf{r}) = \langle\sigma(\mathbf{r})\sigma(\mathbf{r}+\Delta\mathbf{r})\rangle. \tag{20}$$

Inserting the definition of the Fourier transforms and evaluating the mean value of $\exp\{i(\mathbf{q}-\mathbf{q}')\cdot\mathbf{r}\}$ to $\delta_{\mathbf{q}\mathbf{q}'}$, one therefore obtains

$$G_\sigma(\Delta\mathbf{r}) = \sum_{\mathbf{q}} |\tilde\sigma(\mathbf{q})|^2 e^{i\mathbf{q}\cdot\Delta\mathbf{r}}, \tag{21}$$

which reflects nothing but the well-known Wiener-Khin-chine theorem [18, 19]. In full contact, this expression becomes (leaving away the zero-q mode giving an off-set of p_0^2)

$$G_\sigma^{\rm full}(\Delta\mathbf{r}) = \left(\frac{E^*}{2}\right)^2 \sum_{\mathbf{q}} q^2 |\tilde h(\mathbf{q})|^2 e^{i\mathbf{q}\cdot\Delta\mathbf{r}} \tag{22}$$

$$\to -\frac{1}{(2\pi)^2}\left(\frac{E^*}{2}\right)^2 \int d^2q\, q^2 C_{\delta h}(q)\, e^{i\mathbf{q}\cdot\Delta\mathbf{r}} \tag{23}$$

$$= \left(\frac{E^*}{2}\right)^2 \frac{1}{\Delta r}\frac{\partial}{\partial\Delta r}\left\{\Delta r \frac{\partial G_{\delta h}(\Delta r)}{\partial\Delta r}\right\}, \tag{24}$$

where we have used that the multiplication of a Fourier transform with $-q^2$ corresponds to applying the Laplacian to the original function in real space.

2.5. Scale-dependent, mean-square height gradient

A central quantity in Persson theory is the magnification or resolution-dependent mean-square (ms) height gradient. Its definition in a Fourier representation is

$$\bar{g}^2(q) = \sum_{|\mathbf{q}'|<q} q'^2 |\tilde{h}(\mathbf{q}')|^2. \tag{25}$$

A scale-dependent ms height gradient is needed as a function of Δr, in order to formulate a real-space version of Persson theory. We express this as

$$\bar{g}^2(\Delta r) \equiv \frac{1}{(2\pi)^2} \int_0^{2\pi/\Delta r} d^2q\, q^2 C_h(q). \tag{26}$$

The exact evaluation of this term is

$$\begin{aligned} \bar{g}^2(\Delta r) &= \frac{-1}{2\pi} \int d^2\Delta\mathbf{r}' \int_0^{2\pi/\Delta r} dq\, q^3 G_{\delta h}(\Delta r') J_0(q\Delta r') \\ &= \int_0^\infty dx \left\{ J_3(x) - \frac{2J_2(x)}{x} \right\} \frac{G_{\delta h}(x\Delta r)}{\Delta r^2}. \end{aligned} \tag{27}$$

Although this is an analytical expression, it is not practicable, among other reasons because it necessitates a regularizing factor in the integrand. It is therefore numerically more convenient to use eqs. (10) and (26) to deduce the "exact" expression for $\bar{g}^2(\Delta r)$, or, to use approximations.

The simplest approximation to $\bar{g}^2(\Delta r)$ is $4G(\Delta r)/\Delta r^2$, which is asymptotically exact for $q_s \Delta r \ll 1$. However, prefactors are off in the self-affine domain, and incorrect scaling is obtained in the roll-off region. A second, overall better approximation is discussed in Sec. 3.4.

2.6. Partial contact

So far, we have derived expressions for the elastic energy density and the stress ACF. These and related expressions remain exact (within linear elasticity) for partial contact when replacing terms of the form of $|\tilde{h}(\mathbf{q})|^2$ with $|\tilde{u}(\mathbf{q})|^2$,

where $u(\mathbf{r})$ is the true displacement field. The latter differs from the $h(\mathbf{r})$ field whenever contact is partial.

Following the argument by Persson [9, 10] that stress can only be transmitted at those locations, where the elastic manifold appears to be in contact at a resolution of $\lambda = 2\pi/q$, the expectation value $\left\langle |\tilde{\sigma}(\mathbf{q})|^2 \right\rangle$ can be assumed to satisfy

$$\left\langle |\tilde{\sigma}(\mathbf{q})|^2 \right\rangle \approx \left(\frac{qE^*}{2} \right)^2 |\tilde{h}(\mathbf{q})|^2 a_\mathrm{r}(p_0, q). \tag{28}$$

Here, $a_\mathrm{r}(p_0, q)$ is the relative contact area that is obtained when resolving only those spatial features with a wavelength greater $2\pi/q$. In the simplest version of Persson theory, this is approximated as

$$a_\mathrm{r}(p_0, q) \approx \mathrm{erf}\left(\frac{\sqrt{2} p_0}{E^* \bar{g}(q)} \right). \tag{29}$$

Later modifications of the theory include the introduction of a_r-dependent weighting functions $W(a_\mathrm{r})$ (of order unity) on the right-hand side of equation (28) or slightly altered dependencies of a_r on the reduced pressure $p^*(q) \equiv p_0/E^* \bar{g}(q)$.

To use the theory in real space, we need to replace $a_\mathrm{r}(q)$ in the stress ACF with its real-space variant $a_\mathrm{r}(\Delta r)$. This means that the stress ACF in partial contact can be approximated as follows:

$$G_\sigma^\mathrm{part}(\Delta r) \approx p_0^2 + G_\sigma^\mathrm{full}(\Delta r)\ a_\mathrm{r}\left(\frac{p_0}{E^* \bar{g}(\Delta r)} \right), \tag{30}$$

where depending on the required accuracy, either the original expressions for $G_\sigma^\mathrm{full}(\Delta \mathbf{r})$ and $\bar{g}(\Delta \mathbf{r})$ can be used or approximations to them. Likewise, a real-space version of the theory can benefit from empirically determined weighting functions of order unity on the r.h.s of equation (30) or related equations. We will explore this aspect in more detail in the results section.

Assuming that a proper weighting function gives (quasi-) exact results for the stress-ACF, i.e.,

$$G_\sigma^\mathrm{part}(\Delta r) = p_0^2 + G_\sigma^\mathrm{full}(\Delta r) W\{a_\mathrm{r}(\Delta r)\}, \tag{31}$$

we can use the relation

$$\tilde{\sigma}(\mathbf{q}) = \frac{qE^*}{2} \tilde{u}(\mathbf{q}) \tag{32}$$

and the properties of the Fourier transform to deduce correlation functions for the displacement. In principle, it is then possible to write the (quasi-) exact displacement ACF as

$$G_u(r) = \int dr' \int dr'' \hat{K}(r, r', r'')\, G_{\delta h}(r')\, W\{a_\mathrm{r}(r'')\}, \tag{33}$$

where $\hat{K}(r, r', r'')$ is a linear, integro-differential convolution operator with two non-vanishing summands.

At this point, we have only managed to work out a closed-form expression for the simpler summand, which however, we believe to be the most important term when deducing the total elastic energy from the displacement ACF in partial contact conditions. Using only this one summand, we approximate

$$G_{\delta u}(r) \approx G_{\delta h}(r)\, W\{a_\mathrm{r}(r)\}. \tag{34}$$

2.7. Numerical methods

In the result section, we assess the proposed methodology with respect to numerical results. These are either obtained with a house-written Green's function molecular dynamics (GFMD) code or taken from a recently reported contact-mechanics challenge [7].

In the new set of simulations, we do not consider adhesion but only the usual non-overlap constraint as short-range repulsion. Height-spectra are modeled with a continuous transition [21] from the self-affine to the roll-off region via $C_h(q) \propto 1/\{1 + (q/q_\mathrm{r})^2\}^{1+H}$. Two different values of the Hurst exponent are studied, namely $H = 0.5$ and $H = 0.8$. In both cases, the system size is $\mathcal{L} = 16\,\lambda_\mathrm{r}$ and the roll-off wavelength $\lambda_\mathrm{r} = 1024\,\lambda_\mathrm{s}$. The finest discretization in the GFMD simulations satisfied $a = \lambda_\mathrm{s}/32$.

GFMD simulations were run at three different resolutions, each one containing $2^{13} \times 2^{13}$ grid points. All investigated ACFs – in particular height-difference and stress – showed clear overlap when passing from one scale to the next, which turned our sequential multi-scale (or multi-grid) approach into a simple exercise.

In the contact-mechanics challenge, a diverse body of numerical, theoretical and experimental works investigated the adhesive contact of a compliant body

with a computer-generated, albeit typical surface profile. Details of the set-up are described in the original work [7]. Here it shall suffice to say that the physical dimensions were a little smaller than in our new set-up, namely $\mathcal{L}/\lambda_\mathrm{r} = 5$ and $\lambda_\mathrm{r}/\lambda_\mathrm{s} = 200$, however, due to short-range adhesion the discretization of the calculation had to be much smaller than for the new simulations to reach convergence.

3. Results and discussion

3.1. Acquiring $G_{\delta h}(\Delta r)$

Since commercial profilometers do not always provide height-difference ACFs, it might be in place to sketch ways of deducing them from an $h(\mathbf{r})$ measurement. One generic method is to randomly pick initial points on a surface, chose a second point a distance Δr under a random angle, compute the squared height difference between initial and end point and finally average over many such observations. If the spacing between different Δr is taken constant on a logarithmic scale, this procedure scales with $N \ln N$, where $N = \Delta r_\mathrm{max}/\Delta r_\mathrm{min}$. The efficiency of this method should be at least on par with a fast-Fourier-transform based analysis.

It is also possible to acquire $G_{\delta h}(\Delta r)$ by scanning over the surface and by a systematic average over the surface [22, 23]. The numerical cost of deducing $G_{\delta h}(\Delta r)$ from height topographies should not exceed that for generating spectra, since no Fourier or wavelet transform of the data has to be taken. Much can be done to optimize accuracy and efficiency for the computation of a multi-scale correlation function. This, however, is a large topic in itself.

3.2. Advantages of real-space over spectral representations of roughness

While the tribological community is used to consider height spectra, quite a few reasons exist why a real-space based representation bears many advantages. Some of them are:

1. The scale-dependent root-mean-square roughness and gradient can be quickly read off a figure showing $G_{\delta h}(\Delta r)$, which in turn allows for a quick assessment of scale-dependent contact stresses. This point is further elaborated on in sections 3.4 and 3.5.
2. Knowledge of $G_{\delta h}(\Delta r)$ allows one to quickly estimate the elastic energy that is needed to create full contact over a contact patch size of radius a_{c}. This point is discussed in more detail in section 3.6.
3. Experimentally determined profiles may suffer from undesired artifacts, such as erratic spikes as they sometimes arise in weight-light interferometry. Also dimples could be present in a surface. While their precise depth is often irrelevant for contact mechanics, their presence strongly affects the height spectra. The effect of such "undesired" features can be easily eliminated from averaging when acquiring $G_{\delta h}(\Delta r)$ without deteriorating statistics at large Δr, while this is not possible for the determination of $C(q)$ at small q – unless $G_{\delta h}(\Delta r)$ is determined first and $C(q)$ is deduced from it in post processing.
4. When reporting $G_{\delta h}(\Delta r)$ there is no ambiguity with respect to normalizing factors. In contrast, when interpreting $C_h(q)$, the precise choice of the Fourier transform needs to be known, for example. whether a symmetric or asymmetric Fourier transform was used. This point should be irrelevant in an ideal world. However, in our own experience, it takes up a significant amount of time in the initial phases of a collaboration.
5. Since real surfaces are neither infinitely large nor periodically repeated, the Fourier transform needs to be replaced with a wavelet transformation, which can entail information loss, in particular at small and large values of q. To reconstruct $G_{\delta h}(\Delta r)$, it might have to be known what wavelet transformation had originally been used. There is no such ambiguity when reporting $G_{\delta h}(\Delta r)$ to begin with.
6. "Stitching together" measurements using different experimental techniques probing different lengthscales can necessitate quite elaborate considerations [5], while this is quite straightforward to achieve in a real-space

representation.

What could be the advantages for a spectral representation of roughness? At this point, the authors of this paper only see one, namely that Persson theory has so far been formulated in Fourier space. However, first steps are taken in this paper to also formulate it in real space.

3.3. Comparison of real-space versus spectral representations of roughness

It may be instructive to discuss the instantiation of an idealized surface spectrum to better understand the relation between $C_h(q)$ and $G(\Delta r)$. Towards this end, we consider a functional form of a height spectrum as it is often used in numerical studies to approximate the stochastic properties of real surfaces:

$$C_h(q) = C_\mathrm{r} \times \begin{cases} 1 & \text{if } q_\mathrm{r} \leq q < q_0 \\ (q/q_\mathrm{r})^{-2\cdot(1+H)} & \text{if } q_\mathrm{s} \leq q < q_\mathrm{r} \\ 0 & \text{else.} \end{cases} \tag{35}$$

Here, q_s and q_r denote the magnitude of the wave vectors of the short-wavelength and roll-off-wavelength cutoff, respectively. C_r is the value of the spectrum at q_r. The smallest wave vector q_0 can be associated with 2π over the linear system size. The value of the Hurst exponents typically lies between 0.7 and unity [8], however, small values are occasionally reported as well. We therefore chose a compromise, $H = 0.5$, in the numerical example discussed hereafter and note that results for other values of H in the physically meaningful range of $0 < H < 1$ are rather similar, unless H approaches unity, in which case it is difficult to locate the transition from the self-affine to the ballistic scaling regime introduced in Fig. 1.

Fig. 1 shows the height-difference ACF that follows from the idealized spectrum in equation (35) using the parameters $H = 0.5$, $q_\mathrm{s}/q_\mathrm{r} = 10^4$, and $q_\mathrm{r}/q_0 = 10$. $G(\Delta r)$ is normalized to the height variance σ_h and Δr to the inverse roll-off wave vector. The ACF has three domains: The roll-off-region at large Δr, where the surface appears to be flat. The self-affine region, in which $G(\Delta r)$ scales as Δr^{2H} and the short-range region, in which $G(\Delta r)$ scales as Δr^2, which we call

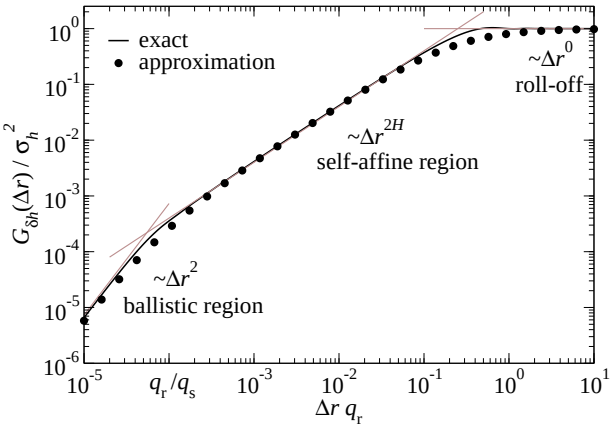

Figure 1: Height-difference ACF $G(\Delta r)$ resulting from the idealized surface-height spectrum given in Eq. (35) using $H = 0.5$ (solid lines). The asymptotic behaviors of three scaling regimes are indicated with gray lines. Circles indicate an approximation to $G_{\delta h}(\Delta r)$ according to equation (36).

the ballistic region in analogy to diffusive processes. It may be difficult or even impossible to observe this latter regime experimentally, since roughness usually extends all the way to (or close to) the atomic scale. However, to describe the contact mechanics of rough surfaces, it can be meaningful to yet approximate surfaces as locally smooth in order to work with a well-defined continuum approach, which can necessitate (unphysical) sub-atomic resolution.

The height-difference ACF produced from equation (35) leads to a functional dependence on Δr, which can be reasonably well approximated with

$$\frac{1}{G_{\delta h}(\Delta r)} \approx \frac{C_{\mathrm{b}}}{\Delta r^2} + \frac{C_{\mathrm{sa}}}{\Delta r^{2H}} + \frac{1}{\sigma_h^2}, \tag{36}$$

which we also expect to be a good representation for experimentally measured profiles. In practice, for example, when an experimentally measured $G_{\delta h}(\Delta r)$ is reported, σ_h, C_{sa}, and H would play the role of adjustable parameters. Although the parameter C_{b} is also a fit parameter, in principle, there will be some ambiguity when determining it in practice for reasons stated in the last

paragraph. In order to yet set C_b, we suggest to chose it such that the reproduced function $G_{\delta h}(\Delta r)$ enters the ballistic regime around a few Angstroms to a nanometer. One reason for this choice is that atomistic simulations indicate a deviation from the possibility of self-affine scaling below one nanometer [24].

When $G_{\delta h}(\Delta r)$ is meaningfully reproduced (its representation might be somewhat approximate near the transition from one regime to another one), the coefficients C_sa and H will ensure that $G_{\delta h}(\Delta r)$ shows the correct scaling behavior in the self-affine regime, while σ_h and C_b take care of the roll-off and ballistic regime, respectively.

A minor oscillation in $G_{\delta h}(\Delta r)$ is noticeable at $\Delta r \approx \lambda_\mathrm{r}$ with a maximum overshoot of 4% from the large Δr asymptotic value of $G(\Delta r)$. It is a consequence of the sharp features in the idealized spectrum, which manifests itself as "ringing", also known as Gibbs phenomenon. If an alternative form for $C_h(q)$ had been chosen for $q > q_\mathrm{s}$, such as $C_h(q) \propto 1/\{1 + (q/q_\mathrm{r})^2\}^{1+H}$, [21] the minor ringing near λ_r would have been suppressed. No ringing becomes obvious near λ_s, despite the hard cutoff at small wave vectors. This, however, can change for higher-order derivatives of $G(\Delta r)$. Similar observations are made for other choices of H. The most important effect is that the ringing at $\Delta r \approx \lambda_\mathrm{r}$ becomes somewhat more visible when H is increased.

Finally, we note that seeing clear transitions between the various regimes in $G_{\delta h}(\Delta r)$ in computer-generated surfaces is not always possible. This is because the linear system size typically ranges from three to four decades with some few simulations being based on $10^5 \times 10^5$ grid points. This is just big enough to see clear scaling in all three regimes. The limitation can be overcome by using sequential multi-scale techniques, e.g., by running simulations at different resolutions and connecting their results – as we do in this paper for our GFMD simulations.

3.4. Assessing scale-dependent height gradients, contact stresses, and contact areas

As discussed in particular in Persson theory, the perceived contact area of nominally flat surfaces depends on the spatial resolution Δr with which the microscopic height fluctuations in a contact are represented; the higher the resolution, the smaller Δr, and the smaller the contact area. In the simplest variant of Persson theory, the relative contact area can be approximated with equation (29). Thus, to estimate scale-dependent contact areas and thus stresses, one first needs to identify scale-dependent surface height gradients $\bar{g}(\Delta r)$.

In order to deduce $\bar{g}(\Delta r)$ from $G_{\delta h}(\Delta r)$, one could use either equation (26) or (27), or, as another and simpler alternative find an approximation to $G_{\delta h}(\Delta r)$ according to:

$$\frac{1}{\bar{g}^2(\Delta r)} \approx \frac{1}{\bar{g}^2(0)} + \frac{C'_{\mathrm{sa}}}{\Delta r^{2(H-1)}} + \left(\frac{\Delta r}{r_{\mathrm{ro}}}\right)^4. \tag{37}$$

The coefficients $\bar{g}(0)$, r_{sa}, H, and r_{ro} can be mostly determined from fits to individual branches of $G_{\delta h}(\Delta r)$. In particular, we find the following relations to be useful

$$\bar{g}^2(0) = 4/C_{\mathrm{b}} \tag{38a}$$

$$C'_{\mathrm{sa}} = c_{\mathrm{sa}}(H) C_{\mathrm{sa}} \tag{38b}$$

$$r_{\mathrm{ro}} = c_{\mathrm{ro}}(H) \sigma_h^2 \lambda_{\mathrm{r}}^2. \tag{38c}$$

Asymptotic estimates for $c_{\mathrm{sa}}(H)$ and $c_{\mathrm{ro}}(H)$ are shown in figure 2. If λ_{r} is not known, it can be associated with the value of Δr above which $G_{\delta h}(\Delta r)$ is roughly constant.

It needs to be kept in mind that the just-mentioned relations may sometimes only provide rough estimates for the scale-dependent $\bar{g}(\Delta r)$, in particular as the precise value of $c_{\mathrm{ro}}(H)$ is somewhat sensitive to how exactly $C(q)$ depends on q near $q_{\mathrm{r}} = 2\pi/\lambda_{\mathrm{r}}$. For example, we find a reduction of $O(40\%)$ in $c_{\mathrm{ro}}(H)$ when the abrupt transition of the self-affine to the roll-off scaling is replaced with a smooth transition [21]. Thus, our approximations are only meant as a recipe for

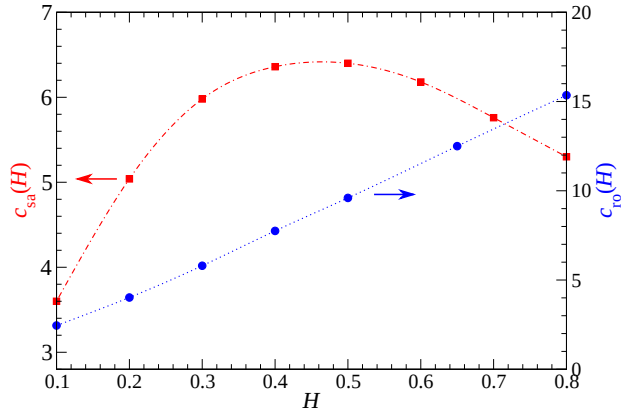

Figure 2: Estimates for the functions $c_{\rm sa}(H)$ (red squares relating to the left ordinate) and $c_{\rm ro}(H)$ (blue circles relating to the right ordinate). Symbols show investigated values of H, while lines are cubic splines through the explicit data.

those who want to take full advantage of the promise made in the last sentence of the abstract of this work.

We now turn our attention to scale-dependent mean contact stresses, which we define as the ratio of external pressure and true contact area at a spatial resolution of Δr:

$$\sigma_{\rm c}(\Delta r) \equiv \frac{p_0}{a_{\rm r}(\Delta r)} \tag{39}$$

$$\approx \frac{E^* \bar{g}(\Delta r)}{\kappa} \text{ for } p_0 \ll E^* \bar{g}(\Delta r). \tag{40}$$

Here, κ is the dimensionless proportionality coefficient relating true contact area and reduced pressure at a small reduced pressure. In the original Persson theory [4], $\kappa = \sqrt{8/\pi}$, while numerical simulations [12, 13, 15, 16, 17], reveal $\kappa \gtrsim 2$ to be a better approximation for randomly rough surfaces satisfying the RPA.

Eq. (40) reveals that the scale-dependent stress is intimately linked to the scale-depend rms gradient, whose spatial dependence we therefore discuss in

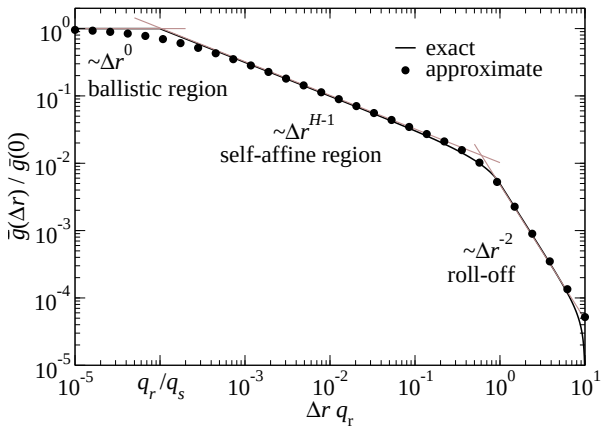

Figure 3: Scale-dependent root-mean-square gradient $\bar{g}(\Delta r)$ for the spectrum defined in equation Eq. (35) using $H = 0.5$ (solid lines). The asymptotic behaviors of three scaling regimes are indicated with gray lines. Circles indicate an approximation to $G_{\delta h}(\Delta r)$ according to equations (37) and (38).

Fig. 3. There, we compare the "exact" dependence of $\bar{g}(\Delta r)$ on Δr with that deduced through fits to $G_{\delta h}(\Delta r)$ and using equation (38)

We conclude this section with a brief discussion of the ramifications of Fig. 3. Assuming that rms-gradients reach the order of unity at the atomic scale of $a_0 \approx 5$ $\mathring{A}$, linear elasticity predicts local contact stresses to be of the order $E^*/2$. This number will not change by much more than an order of magnitude for typical surfaces all the way up to λ_r. To corroborate this claim, we give a numerical example: Assume $H = 0.8$ (which is a quite common value [8]) and $\lambda_\mathrm{r} = 10^5 a_0$. The contact stress is then expected to decrease only by a factor of $(10^5)^{0.2} = 10$ for a description of a resolution with λ_r. For elastomers with a small contact modulus, these numbers are not so large that chemical bonds are broken and the deformation can remain predominantly (visco-) elastic.

In the case of metals, the predicted local scale-dependent elastic stresses much exceed the indentation hardness for all resolutions with $\Delta r < \lambda_\mathrm{r}$. How-

ever, it must be kept in mind that indentation hardness is usually probed with sharp tips leading to large strains and large strain gradients, which enhance plastic deformation. Our brief analysis of the scale-dependence on stress in the previous paragraph and even more so the results on the stress-ACF, presented further below in Sec. 3.7, reveal that the expected (coarse-grained or scale-dependent) elastic stress gradients and thus strain gradients are rather small up to λ_r. This can reduce the amount of plastic deformation predicted by the more detailed strain-gradient-plasticity theories [25] compared to that predicted by scale-independent continuum plasticity. In fact, the displacement of a randomly rough contact turns out smaller with size-dependent plasticity than with continuum plasticity [26] and the trend might somewhat continue to smaller scales when using the more refined discrete-dislocation plasticity (DDP) [27] model. For the parameters (stresses) studied in reference [26], it yet remains unlikely that the most refined treatment would find normal displacements that would be at most $O(10\% - 50\%)$ greater than the ones predicted by linear elasticiy. This means that for sufficiently plastic metals, knowledge of the elastic stress-ACF might be a poor starting point to estimate the amount of plastic deformation.

Our proposition for the estimation of (a lower bound of) the plastic response would yet be to use the smooth shape of $\bar{g}(q)$ – or even better that of the stress ACF – to come up with a first, informed guess for a characteristic, spatial dependence of local stresses. The such obtained stress field can then be used as an initial boundary condition for a DDP analysis. A recently proposed coupling scheme of GFMD and DDP [28] certainly provides an efficient tool for the proposed analysis.

3.5. Quick and dirty assessment of scale-dependent contact stresses

First determine a reasonable guess for H and λ_r by plotting $G_{\delta h}(\Delta r)$ and read off σ_h^2 at $G(\Delta r \to \infty)$.

For $\Delta r < \lambda_\mathrm{r}$:

$$\sigma_\mathrm{sa}(\Delta r) \approx E^* \sqrt{c_\mathrm{sa}(H) G(\Delta r)}/\Delta r \tag{41}$$

For $\Delta r > \lambda_\mathrm{r}$:

$$\sigma_\mathrm{ro} \approx E^* \sqrt{c_\mathrm{ro}(H)} \lambda_\mathrm{r} \sigma_h / \Delta r^2. \tag{42}$$

If you are ambitious, fiddle with λ_r until your estimate of $\sigma(\Delta r)$ is continuous at λ_r. If p_0 exceeds the first estimate of $\sigma(\Delta r)$, take p_0 instead.

3.6. On the Dahlquist criterion

In the derivation of his criterion for tackiness, Dahlquist [29] compared the elastic energy (density) needed to flatten rough surfaces to the energy that is gained upon microscopic contact formation. To evaluate the elastic energy for the Dahlquist criterion, a frequent course of action is to (somehow) estimate a characteristic radius of curvature and amplitude of a single wave. Since most surfaces do not have a distinctive wavelength, the procedure is somewhat ambiguous.

Here, we wish to address a question that is related to the Dahlquist criterion: what is the minimum size of a contact patch that develops when two adhering solids touch in a point? In the absence of external stresses squeezing the two solids against each other, the local contact radius a_c can grow at most until the required elastic energy density exceeds the adhesive energy gain. This leads to the following approximation

$$\gamma \gtrsim v_\mathrm{el}(a_\mathrm{c}) \tag{43}$$

$$\equiv \frac{E^*}{4} \int_0^{a_\mathrm{c}} dr \frac{G_{\delta h}(r)}{r^2}, \tag{44}$$

which is investigated in Fig. 4. The analysis yields an upper estimate for the minimum characteristic contact radius of 18.5 nm for the contact problem that was recently investigated in the contact-mechanics challenge.

A more refined analysis can be based on the assumption that the patch grows as long as its total energy

$$E_\mathrm{patch} \approx a_\mathrm{c}^2 \{-\gamma + v_\mathrm{el}(a_\mathrm{c})\} \tag{45}$$

keeps increasing with the patch radius a_c. This leads to the condition

$$\gamma \approx v_\mathrm{el}(a_\mathrm{c}) + \frac{E^* G_{\delta h}(a_\mathrm{c})}{8 a_\mathrm{c}}, \tag{46}$$

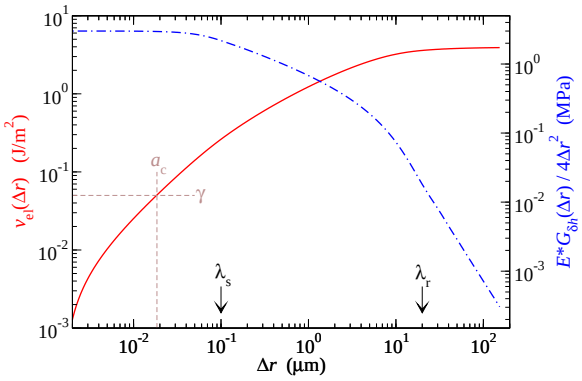

Figure 4: Elastic energy analysis of a self-affine contact (defined in the contact-mechanics challenge [7]). The blue, long-dashed line shows the integrand of the expression yielding the scale-dependent elastic energy $v_{\mathrm{el}}(\Delta r)$ introduced in equation (44). The solid, red line shows $v_{\mathrm{el}}(\Delta r)$. The roll-off λ_{r} and the short wavelength cutoff λ_{s} as well as the areal energy density γ and a first guess for a characteristic minimum contact patch radius a_{c} are indicated by arrows.

which, applied to the data of the contact-mechanics challenge, results in a reduction of our guess for a_{c} to 12.5 nm.

The just-obtained numbers compare well to the minimum characteristic island size observed in the contact-mechanics challenge of $O(1,000\ \mathrm{nm}^2)$ corresponding to a characteristic contact radius of $a_{\mathrm{c}} \approx 17$ nm. We find this agreement quite surprising given the simplicity of the approach, which ignores, among other things, the patchiness of true (non-) contact and the distribution of local contact radii in randomly rough surfaces.

3.7. Stress-autocorrelation function

In the introduction, it was argued why the height-difference ACF contains more useful information for contact mechanics than the Abbott-Firestone curve. In the context of stress fields, one could likewise appreciate that their ACF contains information on how stress decomposes into long and short-wavelength contributions, whereby information on stress gradients is implicitly contained.

In the following, we normalize the stress-ACF to the relative contact area at the smallest scale, i.e., we consider

$$\Gamma_\sigma(\Delta r) \equiv \frac{G_\sigma(\Delta r)}{a_\mathrm{r}(0)}. \tag{47}$$

In the limit $\Delta r \to 0$, $\Gamma_\sigma(\Delta r)$ states the stress variance averaged solely over the true contact, while at large Δr it is essentially the square-root of the stress variance in a contact point times the stress standard deviation a distance Δr away from contact points. We also remind the reader that for small relative contact areas, $\Gamma_\sigma(\Delta r)$ turns out proportional to the contact ACF [30] – except for very small corrections.

We first investigate the full-contact stress ACF in figure 5. Good agreement can be seen between the analytical results and the GFMD data. The $H = 0.5$ curve shows relatively strong Helmholtz ringing for $\Delta r q_\mathrm{s} \approx 1$, which we attribute to the sharp cutoff at $C(q_\mathrm{s})$. Conversely, ringing is more prominent at the transition from the self-affine to the roll-off domain in the $H = 0.8$ system than for $H = 0.5$.

In order to reduce ringing effects in our comparison between GFMD and theory when the pressure is small, we replace $G_\sigma^\mathrm{full}(\Delta r)$ with a function that mimics the exact $G_\sigma^\mathrm{full}(\Delta r)$ quite closely but yet goes smoothly to zero, i.e., at sufficiently large Δr we let the function go to zero with a steep power law. The reason for this choice is that due to the mode coupling between different $\tilde{u}(\mathbf{q})$ at small a_r [31, 32], ringing effects must be expected to smear out, which suppresses sign changes of $G_\sigma^\mathrm{full}(\Delta r)$ at large values of Δr.

In figures 6 and 7, we compare the reduced stress ACF $\Gamma_\sigma(\Delta r)$ obtained at a finite normal stress with GFMD and with two variants of Persson theory. The latter can be described as

$$G_\sigma(\Delta r) = p_0^2 + G_\sigma^\mathrm{full}(\Delta r) W[a_\mathrm{r}\{p^*(\Delta r)\}], \tag{48}$$

where the weighting function satisfies

$$W(a_\mathrm{r}) = \begin{cases} a_\mathrm{r} & \text{original theory} \\ a_\mathrm{ri}^2/a_\mathrm{r} & \text{modified theory} \end{cases} \tag{49}$$

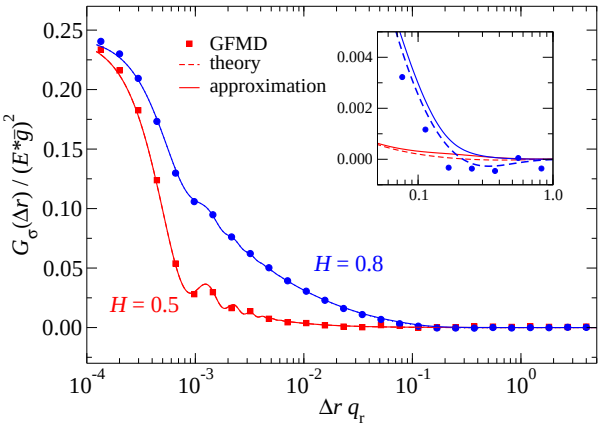

Figure 5: Full-contact stress ACF, $G_\sigma(\Delta r)$, for surfaces with two different Hurst exponents, $H = 0.5$ and $H = 0.8$. Symbols represent GFMD data, thin dashed lines refer to the analytical solution in equation (24), and thick lines to an approximation of the exact stress ACF, which suppresses ringing effects for $\Delta r = O(\lambda_\mathrm{r})$. The inset highlights this latter regime.

Here, a_ri is based on an improved formula for the relative contact area as a function of the reduced (scale-dependent) pressure p^*, closely following equation (15) in reference [32]:

$$a_\mathrm{ri} = \left(1 - a_\mathrm{r}^2\right) \mathrm{erf}(\sqrt{\pi} p^*) + a_\mathrm{r}^3. \tag{50}$$

It is designed such that the a_ri relation satisfies $a_\mathrm{ri} = 2p^*$ at small p^* and smoothly crosses over at intermediate contact areas to the original Persson theory, i.e., equation (29), as full contact is reached. In the modified scheme, we also normalize $\Gamma_\sigma(\Delta r)$ with $a_\mathrm{ri}(\Delta r \to 0)$ in order to divide by our (almost) best possible guess for the relative contact area. The choice of the modified weighting factor is purely heuristic and motivated by our desire to get accurate numbers for $\Gamma_\sigma(\Delta r)$ in the limit $\Delta r \to 0$ and $\Delta r \to \infty$.

Even without the modification to Persson theory, figures 6 and 7 corroborate previous successful tests of the ability of Persson theory to predict the stress ACF for randomly rough surfaces [30]. Here, however, we conduct the analysis

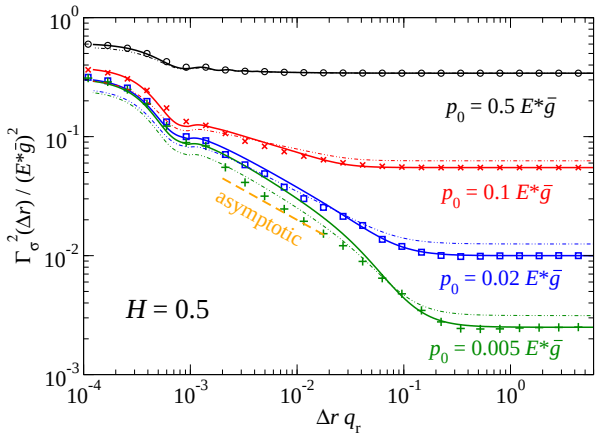

Figure 6: Normalized stress ACF $\Gamma_\sigma(\Delta r)$ for an $H = 0.5$ substrate at various pressures as deduced from GFMD simulations (symbols) and from our real-space interpretation of Persson theory (lines). Thin dashed lines refer to the original unmodified Persson equation, while full lines contain slight modifications to the theory with correction factors of order unity as described in equation (49). The thick dashed lines indicates the low-pressure asymptotics of $\Gamma_\sigma(\Delta r)$ in the self-affine domain, which scales as Δr^{1-H}. Prefactors can be deduced from equation (51). The simulation set-up is described in section 2.7.

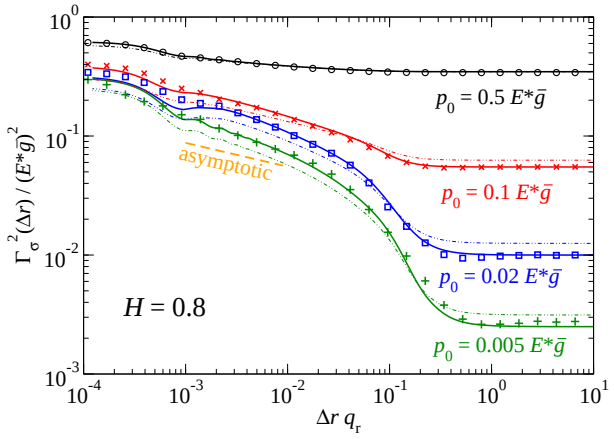

Figure 7: Same as figure 6 except for $H = 0.8$.

in real space rather than in a Fourier representation. We also include the roll-off domain, which had not been considered hitherto in such a stress test of Persson theory. Finally, we find that the simple analytical formula

$$\Gamma_\sigma(\Delta r) = \frac{\pi \bar{g}(\lambda_\mathrm{s}) H^2 E^{*2} \sqrt{G_{\delta h}(\Delta r) c_\mathrm{sa}(H)}}{2\Delta r} \tag{51}$$

provides a quick and yet quite reasonable guess for the asymptotic behavior of the stress ACF in the self-affine scaling regime at small pressures. That scaling behaviour is reflected for only one decade in Δr when representing the self-affine branch with $\lambda_\mathrm{r}/\lambda_\mathrm{s} = O(10^3)$.

4. Conclusions

We demonstrated that the height-difference ACF yields quite useful information on properties that are central to contact mechanics. Not a single of the respective predictions can be even attempted to be made by taking a bearing-area curve as the sole information on the surface topographies. Examples include exact expressions for the elastic energy density and the stress ACF in full contact and approximations of these quantities for partial contact as well as scale-dependent contact stresses within the realm of a real-space interpretation of Persson theory.

When applying the methodology to applications beyond those discussed explicitly in this work, small modification might be necessary. These can be the use of a frequency-dependent contact modulus $E^*(\omega)$ when viscoelasticity becomes important, or, the need to introduce an appropriate scale-dependent $E^*(\Delta r)$ for gradient materials or thin slabs. In the latter case, the term $E^*(\Delta r)$ would have to be pulled into integral expressions like those occurring on the r.h.s. of equation (44).

Our results on partial contacts obtained in the real-space representation turn out as accurately as when Persson theory is conducted in Fourier space. Since our formalism does not require sophisticated mathematics, Fourier transforms, or the writing of elaborate codes but at worst one-dimensional integration or

differentiation with respect to one variable, we hope that the theory might enjoy more wide-spread use than it is currently the case. It remains to be seen what challenges occur when further porting our real-space approach to a broader range of applications, which could include adhesion, plasticity, and predictions on mean gaps as a function of load or gap distribution functions. We are in the process of working out expressions for the scale-dependent elastic energy in partial contact, which will not be quite as elemental as our expressions for scale dependent stresses or the stress ACF. However, we are certain that the only needed mathematical tools remain manipulation of the height-difference ACF in terms of integration and differentiation.

Of course, our formalism does not remedy Persson theory in those situations, where it cannot be expected to lead to accurate results. It will remain flawed when the stress-strain relation differ substantially from linearity or when the surface roughness strongly violates the random-phase approximation. We yet feel that a quick but meaningful analysis of a contact problem within linear elasticity is more useful (even in the mentioned circumstances) than the study of any bearing model neglecting elastic coupling between asperities also because the proper construction of asperity statistics alone is mathematically more demanding and less well defined than the full execution of our formalism. We therefore hope that in the future, height topographies will be routinely reported as height-difference autocorrelation functions rather than as spectra.

Appendix A. Alternative derivation of real-space elastic energy

From dimensional analysis, it is clear that the relation between the height-difference autocorrelation function and the areal elastic-energy density must be of the form

$$v_{\mathrm{el}} = c \cdot E^* \int d\Delta r \frac{G_{\delta h}(\Delta r)}{\Delta r^2}, \tag{A.1}$$

where c is a dimensionless constant, so that units match. We evaluate this expression for single-wavelength roughness as described by

$$h(\mathbf{r}) = \tilde{h}(\mathbf{q}) e^{i\mathbf{q}\cdot\mathbf{r}}. \tag{A.2}$$

With our definition of $h(\mathbf{r})$, the height-difference ACF is

$$G_{\delta h}(\Delta\mathbf{r}) = |\tilde{h}(\mathbf{q})|^2 \{1 - \cos(\mathbf{q} \cdot \Delta\mathbf{r})\} \tag{A.3}$$

and its orientational average

$$\begin{aligned} G_{\delta h}(\Delta r) &= \frac{|\tilde{h}(\mathbf{q})|^2}{2\pi} \int_0^{2\pi} d\varphi \{1 - \cos(q\Delta r \cos\varphi)\} && \text{(A.4)} \\ &= |\tilde{h}(\mathbf{q})|^2 \{1 - J_0(q\Delta r)\}. && \text{(A.5)} \end{aligned}$$

Inserting Eq. (A.5) into Eq. (A.1) and evaluating the integral yields

$$v_{\mathrm{el}} = cE^* q |\tilde{h}(\mathbf{q})|^2. \tag{A.6}$$

The r.h.s. of this equation corresponds to an individual summand in Eq. (12) if $c = 1/4$.

Acknowledgments MHM thanks the Deutsche Forschungs Gesellschaft for financial support through grant Mu-1965/5-1, the Jülich Supercomputing Centre for computing time on JUQUEEN. MHM also thanks David Labonte for bringing the Dahlquist criterion to his attention and Erik van der Giessen for critical feedback.

[1] E. J. Abbott and F. A. Firestone. Specifying surface quality: a method based on accurate measurement and comparison. *Mech. Eng.*, 55:569, 1933.

[2] E.S. Gadelmawla, M.M. Koura, T.M.A. Maksoud, I.M. Elewa, and H.H. Soliman. Roughness parameters. *Journal of Materials Processing Technology*, 123(1):133–145, apr 2002.

[3] A. Majumdar and C. L. Tien. Fractal characterization and simulation of rough surfaces. *Wear*, 136(2):313–327, mar 1990.

[4] B. N. J. Persson. Theory of rubber friction and contact mechanics. *The Journal of Chemical Physics*, 115(8):3840, 2001.

[5] Tevis D B Jacobs, Till Junge, and Lars Pastewka. Quantitative characterization of surface topography using spectral analysis. *Surface Topography: Metrology and Properties*, 5(1):013001, jan 2017.

[6] B.N.J. Persson. Contact mechanics for randomly rough surfaces. *Surface Science Reports*, 61(4):201–227, jun 2006.

[7] Martin H. Müser, Wolf B. Dapp, Romain Bugnicourt, Philippe Sainsot, Nicolas Lesaffre, Ton A. Lubrecht, Bo N. J. Persson, Kathryn Harris, Alexander Bennett, Kyle Schulze, Sean Rohde, Peter Ifju, W. Gregory Sawyer, Thomas Angelini, Hossein Ashtari Esfahani, Mahmoud Kadkhodaei, Saleh Akbarzadeh, Jiunn-Jong Wu, Georg Vorlaufer, András Vernes, Soheil Solhjoo, Antonis I. Vakis, Robert L. Jackson, Yang Xu, Jeffrey Streator, Amir Rostami, Daniele Dini, Simon Medina, Giuseppe Carbone, Francesco Bottiglione, Luciano Afferrante, Joseph Monti, Lars Pastewka, Mark O. Robbins, and James A. Greenwood. Meeting the contact-mechanics challenge. *Tribology Letters*, 65(4), aug 2017.

[8] B. N. J. Persson. On the fractal dimension of rough surfaces. *Tribology Letters*, 54(1):99–106, mar 2014.

[9] B. N. J. Persson. Relation between interfacial separation and load: A general theory of contact mechanics. *Physical Review Letters*, 99(12), sep 2007.

[10] B N J Persson. On the elastic energy and stress correlation in the contact between elastic solids with randomly rough surfaces. *Journal of Physics: Condensed Matter*, 20(31):312001, jun 2008.

[11] B. N. J. Persson and M. Scaraggi. Theory of adhesion: Role of surface roughness. *The Journal of Chemical Physics*, 141(12):124701, sep 2014.

[12] S. Hyun, L. Pei, J.-F. Molinari, and M. O. Robbins. Finite-element analysis of contact between elastic self-affine surfaces. *Physical Review E*, 70(2):026117, aug 2004.

[13] C Campañá and M. H Müser. Contact mechanics of real vs. randomly rough surfaces: A Green's function molecular dynamics study. *Europhysics Letters (EPL)*, 77(3):38005, jan 2007.

[14] Sreekanth Akarapu, Tristan Sharp, and Mark O. Robbins. Stiffness of contacts between rough surfaces. *Physical Review Letters*, 106(20), may 2011.

[15] C. Putignano, L. Afferrante, G. Carbone, and G. Demelio. A new efficient numerical method for contact mechanics of rough surfaces. *International Journal of Solids and Structures*, 49(2):338–343, jan 2012.

[16] Nikolay Prodanov, Wolf B. Dapp, and Martin H. Müser. On the contact area and mean gap of rough, elastic contacts: Dimensional analysis, numerical corrections, and reference data. *Tribology Letters*, 53(2):433–448, dec 2013.

[17] Vladislav A. Yastrebov, Guillaume Anciaux, and Jean-François Molinari. The role of the roughness spectral breadth in elastic contact of rough surfaces. *Journal of the Mechanics and Physics of Solids*, 107:469–493, oct 2017.

[18] Norbert Wiener. Generalized harmonic analysis. *Acta Mathematica*, 55(0):117–258, 1930.

[19] A. Khintchine. Korrelationstheorie der stationären stochastischen Prozesse. *Mathematische Annalen*, 109(1):604–615, dec 1934.

[20] K. L. Johnson. *Contact mechanics*. Cambridge University Press, Cambridge, UK, 1985.

[21] George Palasantzas. Roughness spectrum and surface width of self-affine fractal surfaces via the k-correlation model. *Physical Review B*, 48(19):14472–14478, nov 1993.

[22] Garth J. Simpson, Dana L. Sedin, and Kathy L. Rowlen. Surface roughness by contact versus tapping mode atomic force microscopy. *Langmuir*, 15(4):1429–1434, feb 1999.

[23] R.R.L. De, D.A.C. Albuquerque, T.G.S. Cruz, F.M. Yamaji, and F.L. Leite. Measurement of the nanoscale roughness by atomic force microscopy: Basic principles and applications. In *Atomic Force Microscopy - Imaging, Measuring and Manipulating Surfaces at the Atomic Scale*. InTech, mar 2012.

[24] Soheil Solhjoo and Antonis I. Vakis. Surface roughness of gold substrates at the nanoscale: An atomistic simulation study. *Tribology International*, 115:165–178, 2017.

[25] N.A. Fleck, G.M. Muller, M.F. Ashby, and J.W. Hutchinson. Strain gradient plasticity: Theory and experiment. *Acta Metallurgica et Materialia*, 42(2):475–487, feb 1994.

[26] H. Song, A.I. Vakis, X. Liu, and E. Van der Giessen. Statistical model of rough surface contact accounting for size-dependent plasticity and asperity interaction. *Journal of the Mechanics and Physics of Solids*, 106:1–14, sep 2017.

[27] E. Van der Giessen and A. Needleman. Discrete dislocation plasticity: a simple planar model. *Modelling and Simulation in Materials Science and Engineering*, 3(5):689, 1995.

[28] Syam P Venugopalan, Martin H Müser, and Lucia Nicola. Green's function molecular dynamics meets discrete dislocation plasticity. *Modelling and Simulation in Materials Science and Engineering*, 25(6):065018, aug 2017.

[29] Carl A Dahlquist. An investigation into the nature of tack. *Adhes. Age*, 2:25, 1959.

[30] Carlos Campañá, Martin H Müser, and Mark O Robbins. Elastic contact between self-affine surfaces: comparison of numerical stress and contact correlation functions with analytic predictions. *Journal of Physics: Condensed Matter*, 20(35):354013, aug 2008.

[31] Martin H. Müser. Rigorous field-theoretical approach to the contact mechanics of rough elastic solids. *Physical Review Letters*, 100(5), feb 2008.

[32] Wolf B Dapp, Nikolay Prodanov, and Martin H Müser. Systematic analysis of persson's contact mechanics theory of randomly rough elastic surfaces. *Journal of Physics: Condensed Matter*, 26(35):355002, jul 2014.